Sequential ^1H and ^{15}N NMR Assignments and Secondary Structure of a Recombinant Anti-Digoxin Antibody V_L Domain

Keith L. Constantine, Valentina Goldfarb, Michael Wittekind, James Anthony, Shi-Chung Ng, and Luciano Mueller*

Bristol-Myers Squibb Pharmaceutical Research Institute, P.O. Box 4000, Princeton, New Jersey 08543

Received February 7, 1992

ABSTRACT: A uniformly ^{15}N-labeled recombinant light-chain variable (V_L) domain from the anti-digoxin antibody 26-10 has been investigated by heteronuclear two-dimensional (2D) and three-dimensional (3D) NMR spectroscopy. Complementary homonuclear 2D NMR studies of the unlabeled V_L domain were also performed. Sequence-specific assignments for 97% of the main-chain and 70% of the side-chain proton resonances have been obtained. Patterns of nuclear Overhauser effects observed in 2D NOESY, 3D NOESY–HSQC, and 3D NOESY–TOCSY–HSQC spectra afford a detailed characterization of the V_L domain secondary structure in solution. The observed secondary structure—a nine-stranded antiparallel β-barrel—corresponds to that observed crystallographically for V_L domains involved in quaternary associations. The locations of slowly exchanging amide protons have been discerned from a 2D TOCSY spectrum recorded after dissolving the protein in ^2H_2O. Strands B, C, E, and F are found to be particularly stable. The possible consequences of these results for domain–domain interactions are discussed.

Functional fragments of immunoglobulins, especially of immunoglobulin G (IgG)[1] proteins, have been subject to intensive investigation in recent years. This is due to the potential advantages that such fragments may offer in practical applications (Colcher et al., 1990; Chaudhary et al., 1989; Ward et al., 1989; Bird et al., 1988) and to the advantages they offer for detailed study of structure, dynamics, and function. In particular, individual immunoglobulin domains ($M_r \sim 12.5$K) and covalently or noncovalently associated domain pairs are suitable for detailed study using recently developed heteronuclear multidimensional NMR methods (Mueller et al., 1992; Fesik & Zuiderweg, 1990; Kay et al., 1990).

The Fv fragment, which is a heterodimer produced by the noncovalent association of the V_H and V_L domains, is the smallest IgG fragment which contains a complete antigen binding site (Givol, 1991). NMR studies of recombinant (McManus & Reichmann, 1991; Wright et al., 1990) and monoclonal antibody-derived (Takahashi et al., 1991) Fv fragments have recently been reported. These investigations focused primarily on NMR assignments relevant to antigen–antibody interactions. In addition to NMR experiments, Fv fragments have been studied by other techniques. A crystallographic investigation of the Fv from the anti-lysozyme antibody D1.3 has been reported (Bhat et al., 1990); this study revealed very similar conformations and antigen contacts for Fv and Fab structures. Various strategies for stabilizing Fv fragments via covalent linkage of the V_H and V_L domains have been examined (Glockshuber et al., 1990). These strategies include the construction of single-chain Fv proteins (Pantoliano et al., 1991; Huston et al., 1988; Bird et al., 1988), in which the domains are linked by an inserted peptide segment. Recently, Fv versions of catalytic antibodies have been produced (Gibbs et al., 1991; Baldwin & Schultz, 1989).

Although they lack complete antigen binding sites, V_H and V_L domains separated from their respective V_L and V_H partners may, in some instances, retain significant binding activity, either as monomers (Ward et al., 1989) or as homodimers (Edmondson et al., 1984). In a unique case, the light chains of a group of polyclonal catalytic antibodies were found to have substantially greater catalytic activity than the parent Fabs (Mei et al., 1991). These results strongly suggest that separated domains generally have conformations that are the same or very similar to those found in the larger fragments. Thus, in cases where the individual domains retain some functional activity, opportunities for dissecting antibody–antigen interactions present themselves. Study of isolated V_H and V_L domains is also of interest in regard to domain–domain interactions (see below).

The Fv fragment of the anti-digoxin antibody 26-10 has been expressed in *Escherichia coli*, both as a single-chain Fv (Huston et al., 1988) and as individual V_H and V_L domains (Anthony et al., 1992). The noncovalent Fv (henceforth, simply Fv) and the isolated V_L domain were found to be soluble, whereas the isolated V_H domain precipitates at concentrations required for NMR studies. A crystal structure at 2.5-Å resolution of the 26-10 Fab complexed with the cardiac glycoside digoxin has been described (Jeffrey et al., unpublished results). The F_v binds digoxin with high affinity (1.3×10^9 M^{-1}) (Anthony et al., 1992). The affinities of native and mutant 26-10 antibodies for a number of digoxin analogues have been determined (Schildbach et al., 1991). These data indicate that the 26-10 Fv should provide an ideal system for NMR studies of antigen–antibody interactions.

The isolated 26–10 V_L domain does not retain detectable digoxin affinity. However, the 26–10 V_L is of interest with regard to its relatively high affinity for the V_H domain. The 26-10 Fv has a >48-h half-life for domain–domain dissociation

* To whom correspondence should be addressed.

[1] Abbreviations: C_{H1}, constant domain 1 of the heavy chain; C_L, constant domain of the light chain; CDR, complementarity determining region; DQF-COSY, 2D double-quantum-filtered correlation spectroscopy; Fab, antigen binding fragment composed of the C_{H1}, C_L, V_H, and V_L domains; FID, free induction decay; FPLC, fast performance liquid chromatography; FR, framework region; Fv, antibody fragment composed of the V_H and V_L domains; HSQC, heteronuclear single-quantum coherence; IgG, immunoglobulin G; NOE, nuclear Overhauser effect; NOESY, NOE spectroscopy; t_m, mixing time; TOCSY, total correlation spectroscopy; TSP, (trimethylsilyl)[2,2,3,3-$^2H_4$]propionate; V_H, variable domain of the heavy chain; V_L, variable domain of the light chain; 1D, one-dimensional; 2D, two-dimensional; 3D, three-dimensional.

0006-2960/92/0431-5033$03.00/0

at 37 °C and a V_H/V_L dissociation constant $<10^{-7}$ M (Anthony et al., 1992). This is in marked contrast to the Fv fragment of the phosphocholine binding antibody McPC603, for which the half-life for domain–domain dissociation and the V_H/V_L dissociation constant at 37 °C are 1.3 h and $\sim 10^{-6}$ M, respectively (Glockshuber et al., 1990). Thus, 26-10 may serve as a useful model system to determine the factors responsible for relatively stable V_H/V_L association. To accomplish this goal, a detailed study of any conformational or dynamic changes which occur upon domain–domain association is required in addition to characterization of the domain–domain interactions observed in the Fv fragment itself.

Assignments of the backbone ^1H resonances have been obtained for 110 of the 113 residues in the 26-10 V_L domain. Unambiguous assignments for 70% of the side-chain ^1H resonances were also obtained. Features of secondary structure were characterized on the basis of observed patterns of sequential, medium-range, and long-range NOEs, on the identification of slowly exchanging backbone HN protons, and estimated $^3J_{\alpha HN}$ couplings constants. At this qualitative level, no obvious difference between secondary structure features of the V_L domain in solution and the V_L domain within the Fab crystal structure could be discerned. These studies demonstrate that no major rearrangements of the V_L domain secondary structure occur upon association with the V_H domain, complexation with digoxin, or crystallization. On the basis of hydrogen exchange data, high stability for β-strands B, C, E, and F is found. These results lay the groundwork necessary for detailed characterization of the solution structure and dynamics of the 26-10 V_L domain, both in isolation and as part of the Fv.

Materials and Methods

Protein Purification and Sample Preparation. The 26-10 V_H and V_L domains have been expressed in *Escherichia coli* strain JM109/DE3. Details on the plasmid construction and expression conditions are described elsewhere (Anthony et al., 1992). The induced cells express the V_L domain to a much higher level than the V_H domain, in both rich and minimal media. This results in the accumulation of a significant amount of unassociated V_L domain in the periplasm in addition to the Fv fragment. The V_L domain was purified by essentially the same methods that were used to purify the Fv fragment (Anthony et al., 1992), except that two additional chromatography steps were employed.

Cells were grown on 2×YT media to obtain unlabeled protein or on minimal media with [^{15}N]ammonium sulfate to obtain ^{15}N-labeled V_L domain. The cells were harvested and osmotically shocked to release proteins contained within the periplasmic space. Precleared osmotic shock supernatant was applied to a ouabain–Sepharose affinity column to remove the Fv fragment, which binds ouabain. The flow-through protein fraction containing the V_L domain was dialyzed against 10 mM Tris-HCl (pH 8.0) and passed through Macro-Prep 50 Q resin (Bio-Rad); this latter step reduced contaminating proteins by ~80%. Unbound proteins were concentrated on an Amicon concentrator, dialyzed against 10 mM NaOAc (pH 6.5), and applied to a Mono S10/10 column (FPLC, Pharmacia), and the V_L domain was eluted with a 0–300 mM NaCl gradient. Fractions containing the protein were combined and analyzed for purity by SDS–PAGE. Protein concentrations were determined by the BCA method (Pierce).

Protein samples for NMR measurements (0.50 mL) were concentrated into buffers containing 50 mM deuterated NaOAc, 0.001% NaN_3, and 99.96% ^2H_2O (unlabeled sample only) or 90%/10% (v/v) $H_2O/^2H_2O$ (unlabeled and uniformly ^{15}N-labeled samples). The pH values were adjusted to 5.5 (measurements were not corrected for ^2H isotope effects). For preparation of the 99.96% ^2H_2O sample, the protein was lyophilized to a dry powder and then redissolved in the buffer. The protein concentration of the ^{15}N-labeled sample was ~3.4 mM.

NMR Spectroscopy. NMR experiments were recorded at 30 °C using a Varian UNITY-600 spectrometer operating at 599.9 and 60.8 MHz for ^1H and ^{15}N, respectively. Homonuclear ^1H spectra were acquired with a ^1H probe, while heteronuclear ^1H–^{15}N spectra were recorded using a ^1H–^{13}C–^{15}N triple-resonance probe. Spectral widths in the ^1H dimension(s) were 9000 and 10 000 Hz for samples dissolved in 99.96% ^2H_2O and 90%/10% $H_2O/^2H_2O$, respectively, and for heteronuclear experiments, the ^{15}N spectral width was 2000 Hz. For ^1H, chemical shifts (δ) were referenced to an external TSP standard. The ^1H carrier was placed on the H_2O or residual H^2HO resonance (4.78 ppm). For homonuclear spectra, the water resonance was suppressed by low-power presaturation during the recycle delay (1.2–1.5 s), while for heteronuclear spectra the SCUBA sequence (Brown et al., 1988) followed presaturation. The ^{15}N carrier frequency was set to 120.0 ppm, and the WALTZ-16 sequence (Shaka et al., 1983) was used for ^{15}N decoupling during ^1H acquisition.

For 2D homonuclear spectra, 400 or 512 equally spaced complex t_1 experiments were recorded. Each FID (32 signal-averaged transients) consisted of 4096 complex points in t_2. Acquired 2D homonuclear data included DQF-COSY (Rance et al., 1983), clean TOCSY (Griesinger et al., 1988; Bax & Davis, 1985; Braunschweiler & Ernst, 1983), and NOESY (Bodenhausen et al., 1984; Kumar et al., 1980; Macura & Ernst, 1980) spectra. For these phase-sensitive experiments, quadrature detection in both dimensions was achieved via the hypercomplex method (States et al., 1982; Mueller & Ernst, 1979). Mixing times (t_m) of 50 and 70 ms were used for the TOCSY spectra, and NOESY data were acquired with t_m of 50 and 200 ms. For the NOESY experiments, solvent peak recovery was reduced by inclusion of a 180° composite pulse in the center of the mixing period.

A 2D ^{15}N–^1H HSQC spectrum (Bodenhausen & Ruben, 1980) was recorded as 164 t_1 increments, with 64 scans per increment and 1024 complex points in t_2. Hypercomplex data acquisition was used in the F_1 (^{15}N) dimension. All 3D spectra were recorded as ^{15}N single-quantum variants (Norwood et al., 1990). These included TOCSY–HSQC, NOESY–HSQC, TOCSY–NOESY–HSQC, and NOESY–TOCSY–HSQC experiments (Mueller et al., 1992). Correlations observed by the latter two methods are the result of two consecutive transfer steps. NOESY and TOCSY t_m values used were 120 and 60 ms, respectively, for all 3D spectra.[2] The hypercomplex data were collected at 128 complex × 32 complex × 1024 complex points in the F_1, F_2 (^{15}N), and F_3 dimensions, respectively.

NMR spectra were processed with the FELIX program (Hare Research, Inc.) running on a Silicon Graphics 4D/240 VGX computer. For all experiments, low-frequency deconvolution (Marion et al., 1989) was applied to the acquisition dimension to remove the water signal. Homonuclear 2D spectra were Fourier-transformed to produce matrices consisting of 2048 × 2048 real data points. Prior to transformation, the first complex point of each time domain was halved to reduce

[2] For consistency, all TOCSY mixing periods used for the 3D experiments were kept relatively long (60 ms) to emphasize weak couplings. Ideally, 3D TOCSY–NOESY–HSQC and NOESY–TOCSY–HSQC experiments should also be recorded with shorter TOCSY mixing times (30–40 ms) to minimize sensitivity loss (Mueller et al., 1992).

base-plane artifacts (Otting et al., 1986). Also before transformation, the 2D NOESY data were multiplied by a Gaussian window function in t_2 and a 50°-shifted skewed sine-bell window function in t_1. 2D TOCSY spectra were processed with Gaussian apodization in both dimensions, and 2D DQF-COSY spectra were processed with 30°-shifted sine-bell windows in both dimensions.

The 2D ^{15}N–^1H HSQC spectrum was multiplied by a 70°-shifted skewed sine-bell in t_2 and a 90°-shifted sine-bell in t_1; it was subsequently Fourier-transformed into a 512 real × 512 real matrix. The 3D heteronuclear spectra were processed to yield frequency domain matrices consisting of 512 real × 64 real × 256 real data points in F_1, F_2, and F_3, respectively. The time domain data were multiplied by a 70°-shifted skewed sine-bell in t_3, a 70°-shifted sine-bell in t_2, and a 90°-shifted sine-bell in t_1. The first complex t_2 data point was replaced by a back-predicted point produced by complex linear prediction (L. Kay and M. Friedrichs, unpublished results), and the t_2 data were extended forward by 30 points, also by complex linear prediction, prior to Fourier transformation. For all heteronuclear spectra, the upfield half of the ^1H acquisition dimension was discarded.

Standard geometry ^1H coordinates were built onto the 26-10 V_L domain structure derived from the 26–10 Fab X-ray coordinates (Jeffrey et al., unpublished results) using the XPLOR program (Brunger, 1990). All distances that were <5.0 Å and involved only HN of H^α atoms were extracted and used to confirm observed sequential, medium-range, and long-range backbone proton NOEs.

Results and Discussion

Preliminary Characterization. The results of FPLC analysis indicate that the isolated 26-10 V_L domain is monomeric when applied to the column (Pharmacia, Superose 12) at an initial protein concentration of ~3.0 mM. 1D ^1H NMR spectra recorded at 30 °C revealed no detectable changes in the line widths or chemical shifts for protein concentrations between 0.7 and 3.4 mM. An NMR-monitored thermal melting study of a 0.7 mM sample of unlabeled V_L domain demonstrated that the protein denatures between 50 and 60 °C.

Antibody light chains and V_L domains are known to dimerize (Stevens et al., 1991); however, their association constants vary from $<10^3$ to $>10^6$ M^{-1} (Stevens et al., 1980). The existence of monomeric light chains (Mei et al., 1991; Stevens et al., 1980; Kishida et al., 1975) and V_H domains (Ward et al., 1989) has been demonstrated. This lends support to our finding that the 26-10 V_L domain exists predominantly as a stable monomer under the conditions employed in this study.

Spin System Identification. The ^{15}N–^1H HSQC spectrum serves as the starting point for spin system identification. Figures 1 and 2 show the upfield and downfield ^{15}N regions of this spectrum, respectively. Backbone HN cross-peaks are labeled with the sequential identifications derived below. An initial analysis of the HSQC spectrum revealed 98 backbone HN cross-peaks (106 expected), 1 Trp side-chain H^1N cross-peak (1 expected), 20 Asn side-chain $H^\delta N$ or Gln side-chain $H^\epsilon N$ cross-peaks (20 expected), and 4 folded Arg–side–chain $H^\epsilon N$ cross-peaks (5 expected). The locations of the folded cross-peaks were unambiguously established by recording a second ^{15}N–^1H HSQC spectrum with a sweep width in the ^{15}N dimension of 4000 Hz. Also, 5 of the backbone HN cross-peaks each involve 2 nearly completely overlapped cross-peaks, bringing the total number of backbone HN cross-peaks observed in the HSQC spectrum to 103.

A number of side-chain spin systems were initially identified from the 2D homonuclear spectra. The ring ^1H resonances

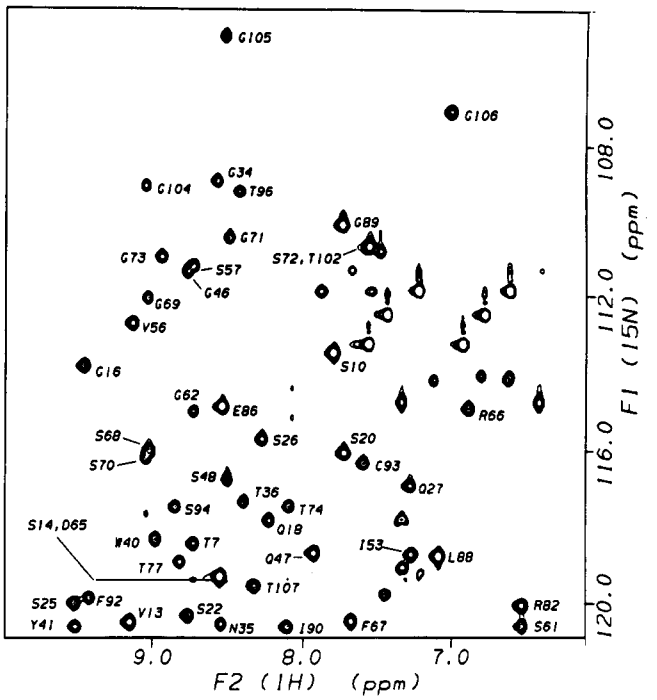

FIGURE 1: 600-MHz 2D ^{15}N–^1H HSQC spectrum of the 26-10 V_L domain: upfield ^{15}N region. Cross-peaks arising from backbone amide groups are labeled. The spectrum was recorded at 30 °C on a 3.4 mM V_L sample dissolved in 90%/10% (v/v) $H_2O/^2H_2O$ containing 50mM deuterated NaOAc/0.001% NaN_3, pH 5.5.

of the single Trp residue (Trp^{40}) were readily located in the 2D TOCSY and DQF-COSY spectra; these resonances were connected to the Trp^{40} polypeptide backbone spin system via intraresidue cross-peaks observed in the 2D NOESY spectra. Both His ring spin systems, three out of four Tyr ring spin systems, and two out of five Phe ring spin systems were identified and subsequently linked to their corresponding backbone fragments. At least partial spin system identification was achieved for 11 of 19 Leu or Val residues, 3 out of 5 Ile residues, 9 our of 11 Gly residues, 6 out of 16 Ser residues, 8 out of nine Thr residues, and 2 out of 3 Ala residues.

The backbone HN spin system located in the HSQC spectrum was correlated with H^α and side-chain protons by inspection of the F_1 and F_3 planes of the 3D TOSCY–HSQC spectrum. An example is shown in Figure 3A, which shows slices of the 3D TOCSY–HSQC spectrum containing cross-peaks identifying the Val^2, Val^3, Met^4, Thr^5, Gln^6, and Thr^7 spin systems. (The sequential assignment of these residues is discussed below.) When possible, side-chain systems identified in this way were matched to those located in the 2D homonuclear spectra. Proceeding in this manner, backbone spin systems were correlated to specific residue types for 3 Val, 6 Thr, 8 Gly, 10 Ser, 1 Ala, 2 Ile, 3 Leu, and 2 Arg residues and for the aromatic residues mentioned above. In addition, examination of NOEs in the 3D NOESY–HSQC spectrum involving side–chain protons bonded to ^{15}N afforded identifications for the backbone and side-chain spin systems for five Asn or Gln residues. The remaining spin systems were classified as belonging to long side chains if connectivities past the H^β and $H^{\beta'}$ resonances were observed. Due to inefficient transfer of magnetization, relayed cross-peaks were not always present for long side chains. Thus, unambiguous classification of spin systems into the short side-chain category was not feasible. The identified spin systems provided the basis for the sequential assignment procedure (Wuthrich, 1986).

Sequential Assignments and Secondary Structure. The general conformation of antibody V_L domains is well-known

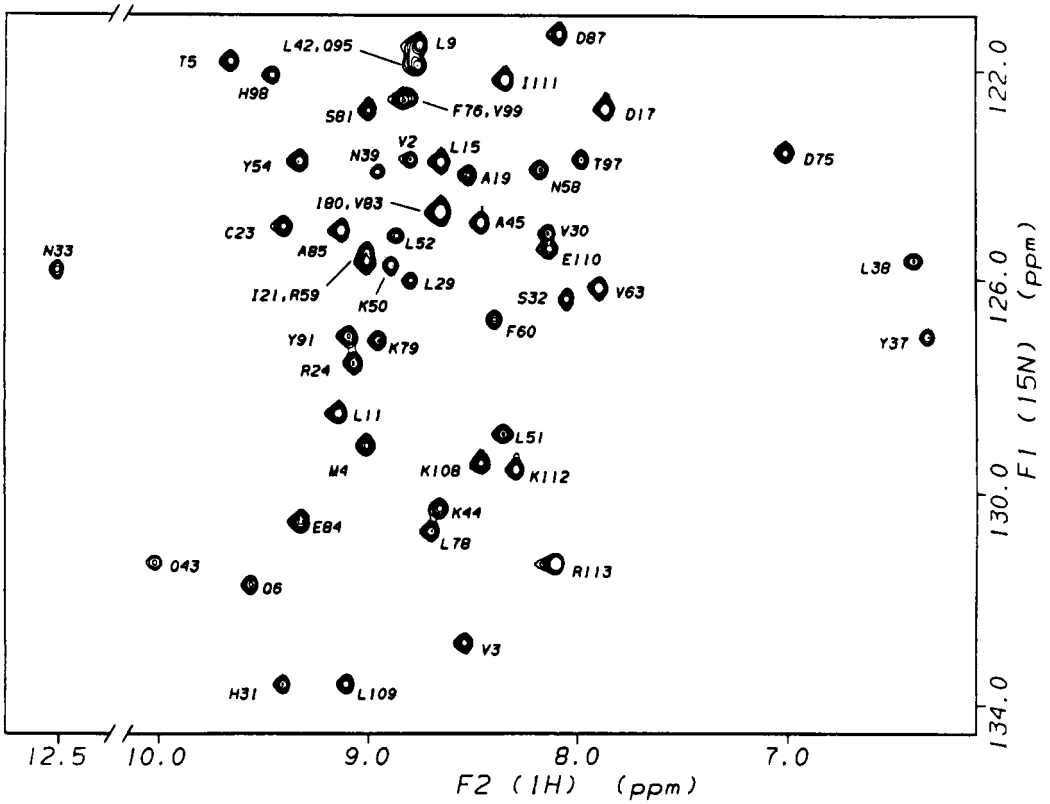

FIGURE 2: 600-MHz 2D ^{15}N–^{1}H HSQC spectrum of the 26-10 V_L domain: downfield ^{15}N region. The region containing the Trp^{40} H^1N cross-peak (δ H^1N = 11.04 ppm) is not shown. See the caption of Figure 1 for additional details.

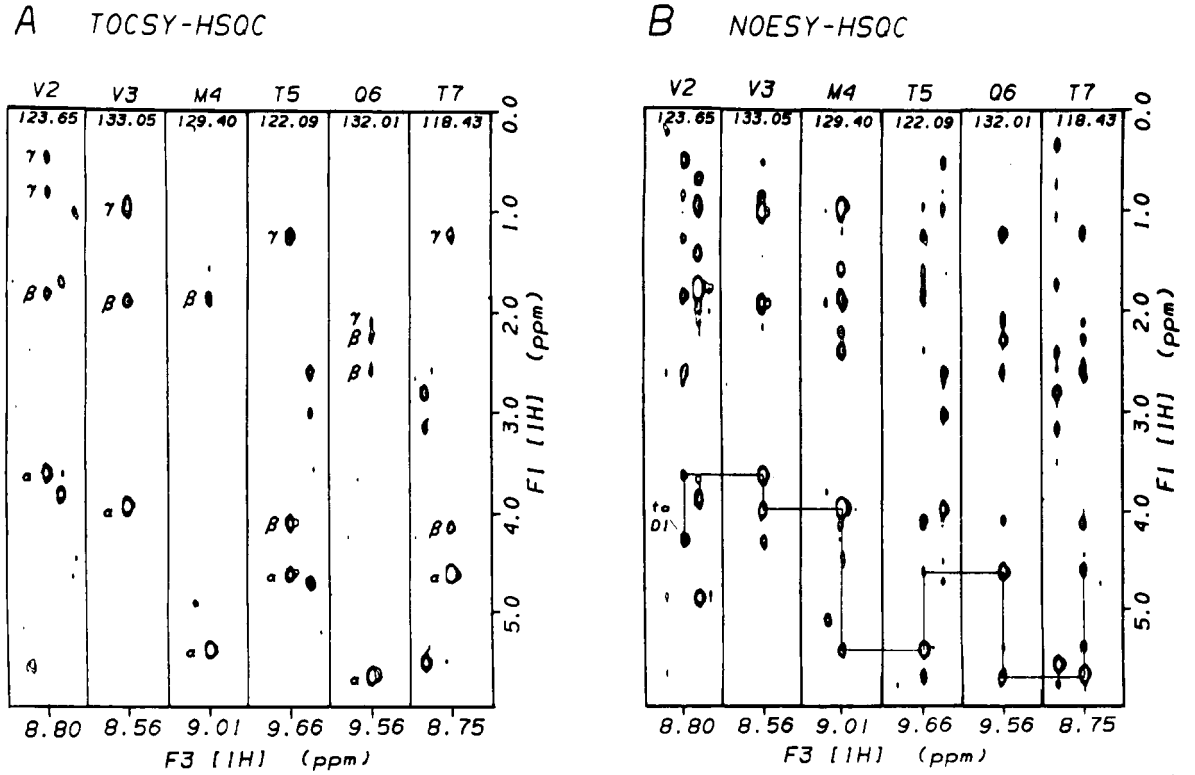

FIGURE 3: F_3, F_1 planes of 600-MHz 3D spectra showing HN–aliphatic connectivities involving the HN resonances of Val^2 through Thr^7. The ^{15}N chemical shift of each plane is given near the top of each slice, and the HN chemical shifts are indicated along the F_3 dimension. (A) Slices of the 3D TOCSY–HSQC spectrum. Intraresidue cross-peaks are denoted by Greek letters corresponding to the identity of the aliphatic proton resonance along the F_1 dimension. (B) Slices of the 3D NOESY–HSQC spectrum. The pathway of sequential $d_{\alpha N}$ connectivities is traced with a solid line. Experimental conditions are the same as for Figure 1.

from X-ray crystallography [for reviews, see Davies et al. (1990) and Colman (1988)]. The domain consists of a nine-stranded antiparallel β-barrel, with the strands designated A, B, C, C′, C″, D, E, F, and G. Loops connecting strands B to C, C′ to C″, and F to G form complementarity determining regions (CDRs) 1, 2, and 3, respectively. These loops, together with their V_H domain analogs, comprise the antibody combinding site. The β-sheet secondary structure is expected

to yield strong sequential $d_{\alpha N}$ NOE connectivities, weak or absent sequential d_{NN} connectivities, and weak intraresidue $d_{\alpha N}$ NOE connectivities (Wuthrich, 1986). Interresidue $d_{\alpha N}$, $d_{\beta N}$, and d_{NN} connectivities were identified from examination of the 3D TOCSY–HSQC and NOESY–HSQC spectra. The identities of the spin systems involved in d_{NN} NOE connectivities were established as follows. Consider a d_{NN} cross-peak observed in the ^{15}N plane of a particular spin system (denoted spin system A) involving the HN resonance of spin system A (F_3 coordinate) and the HN resonance of a second spin system B (F_1 coordinate). For such situations, the ^{15}N plane of spin system B (and thus its identity) was deduced by examining a 1D vector along the ^{15}N dimension at the symmetric F_1, F_3 position. This vector passes through the symmetric cross-peak in ^{15}N plane spin system B. The identity of spin system B was subsequently confirmed by plotting its corresponding ^{15}N plane and locating the d_{NN} cross-peak to spin system A.

Sequential $d_{\alpha N}(i,i+1)$ connectivities are observed in the ^{15}N plane of the $i+1$ spin system. In these cases, the identity of spin system i is often ambiguous due to overlap of H^{α} resonances. For these situations, the identity of spin system i was established by examination of $d_{\beta N}$ connectivities, and by analysis of the 3D TOCSY–NOESY–HSQC and NOESY–TOCSY–HSQC spectra, as described in more detail below. In concert with the sequential assignments, the characteristic NOEs which define β-strand contacts (Wuthrich, 1986) were identified in the 2D NOESY, 3D NOESY–HSQC, and 3D NOESY–TOCSY–HSQC spectra. All observed $d_{\alpha N}$ and d_{NN} connectivities were checked against those expected on the basis of the 26-10 Fab X-ray structure (Jeffrey et al., unpublished results).

Figure 3B shows an example sequential connectivity pathway involving residues Val^2 through Thr^7. Slices through the 3D NOESY–HSQC spectrum reveal an unbroken stretch of strongh sequential $d_{\alpha N}$ cross-peaks between these residues. Numerous $d_{\beta N}$ NOEs are also observed. The locations of the Asp^1 H^{α} and H^{β} resonances are evident from NOEs to the Val^2 HN resonance. In addition, slow H-exchange is observed for Thr^5; i.e., the HN resonance was present in a 2D TOCSY spectrum recorded between 12 and 24 h after the protein was dissolved in 99.96% ^2H_2O. Large (>8 Hz) $^3J_{\alpha HN}$ coupling constants were roughly estimated from cross sections through the 2D DQF-COSY spectra for Met^4, Thr^5, Gln^6 and Thr^7. This combined information clearly demonstrates that Val^2 through Thr^7 adopts an extended conformation. This is completely consistent with the known X-ray structure, as these residues form the N-terminal half of strand A. The stretch of strong sequential $d_{\alpha N}$ connectivities is broken by the occurrence of a Pro residue at position 8.

The utility of the 3D TOCSY–NOESY–HSQC and NOESY–TOCSY–HSQC spectra for establishing the identity of spin system i for strong $d_{\alpha N}(i,i+1)$ connectivities is illustrated by the data presented in Figure 4. Figure 4A shows the HN–HN region of the NOESY–HSQC ^{15}N plane (120.0 ppm) which contains the F_3, F_1 diagonal peaks for Ser^{25} HN and Phe^{92} HN. Neither of these resonances is involved in d_{NN} connectivities. Both, however, are involved in strong $d_{\alpha N}$ connectivities with the preceding (i) residues (not shown). The locations of the HN resonances of these residues (Arg^{24} and Tyr^{91}) are revealed by the F_1 positions of cross-peaks which appear in the 120.0 ppm ^{15}N plane of the TOCSY–NOESY–HSQC spectrum (Figure 4B). These peaks are produced by a TOCSY transfer of magnetization from the NH resonance of residue i (F_1) to the H^{α} resonance of residue i, followed by NOESY transfer to the HN resonance of residue $i+1$ (F_3). In this particular case, both residue i NH resonances occur at ~9.1 ppm. The ^{15}N planes of the i residues can be established by examination of the NOESY–TOCSY–HSQC spectrum. HN–HN cross-peaks are produced by NOESY transfer from the HN resonance of residue $i+1$ (F_1) to the H^{α} resonance of residue i, followed by TOCSY transfer to the HN resonance of residue i (F_3). This is illustrated by Figure 4C,D for Arg^{24} and Tyr^{91}, respectively. The backbone ^{15}N resonance for Arg^{24} is located in the 127.83 ppm plane, and for Tyr^{91}, the resonance is in the 127.31 ppm plane. These are adjacent planes in the NOESY–TOCSY–HSQC spectrum. The clean separation observed is a reflection of the enhanced resolution afforded by ^{15}N single-quantum coherence over multiple-quantum coherence (Norwood et al., 1990), and by the use of linear prediction data extension in the F_2 dimension.

A summary of observed sequential and $i,i+2$ connectivities is presented in Figure 5. The locations of slowly exchanging HN protons and residues with $^3J_{\alpha HN} > 8$ Hz are also displayed. (Due to limited sensitivity of the 2D DQF-COSY spectra, residues other than those indicated in Figure 5 may also have $^3J_{\alpha HN} > 8$ Hz.) As expected, strong sequential $d_{\alpha N}$ connectivities are predominant. These data afforded assignments for the backbone protons of all but three of the residues in the 26-10 V_L domain. Assigned resonance positions are reported in Table I. Ser^{28}, Lys^{55}, and Pro^{100} remain unassigned. ^{15}N–^1H correlations have not been located in the 2D HSQC spectrum for Ser^{28} or Lys^{55}. It is noteworthy that both of these residues reside in CDR regions—Ser^{28} is in CDR1, which extends from Gln^{27} to Asn^{39}, and Lys^{55} is in CDR2, which encompasses Lys^{55} through Ser^{61}. Thus, these resonances may be absent due to rapid exchange with the solvent protons or, what is more likely, due to line broadening induced by conformational change. Several additional potential amino acid spin systems have been identified by the appearance of weak cross-peaks in the 3D TOSCY–HSQC spectrum. However, none of these potential spin systems yield connectivities which identify Ser^{28} or Lys^{55}. We note that one such spin system has been identified as Phe^{103}, which does not give rise to a detectable cross-peak in the 2D HSQC spectrum. This residue is adjacent to CDR3, which runs from Ser^{94} to Thr^{102}.

Pro residues were generally identified by observation of $d_{\alpha N}$ connectivities involving the HN resonance of the following residue. This was not possible for Pro^{100}, as it is followed by Pro^{101}. The Val^{99}–Pro^{100} peptide bond is expected to be cis (P. Jeffrey, personal communication). Thus, a strong H^{α}–H^{α} NOE should arise between these residues (Wuthrich, 1986). However, the expected NOE could not be identified unambiguously. Another region of the sequence which proved rather difficult to assign was the stretch containing CDR2 residues Ser^{57} through Phe^{60}. The H^{α} resonances of all four of these residues fall between 4.67 and 4.69 ppm (Table I). Thus, sequential $d_{\alpha N}$ NOEs were initially mistaken for intraresidue NOEs. These residues were assigned by reference to the X-ray structure, by inspection of 3D NOESY–TOCSY–HSQC and TOCSY–NOESY–HSQC spectra as described above, and by elimination.

Overall, the sequential and $i,i+2$ connectivities observed for the isolated 26-10 V_L domain in solution reflect those expected on the basis of the 26-10 Fab X-ray structure. The main exceptions to this trend occur in the CDR regions, where a number of expected NOEs are absent or occur at a reduced intensity. The expected medium-intensity sequential $d_{\alpha N}$ connectivities between Ser^{32}, Asn^{33}, and Gly^{34} are absent, and the corresponding d_{NN} connectivities, which are expected to have medium–strong intensities, are weak. The sequential $d_{\alpha N}$

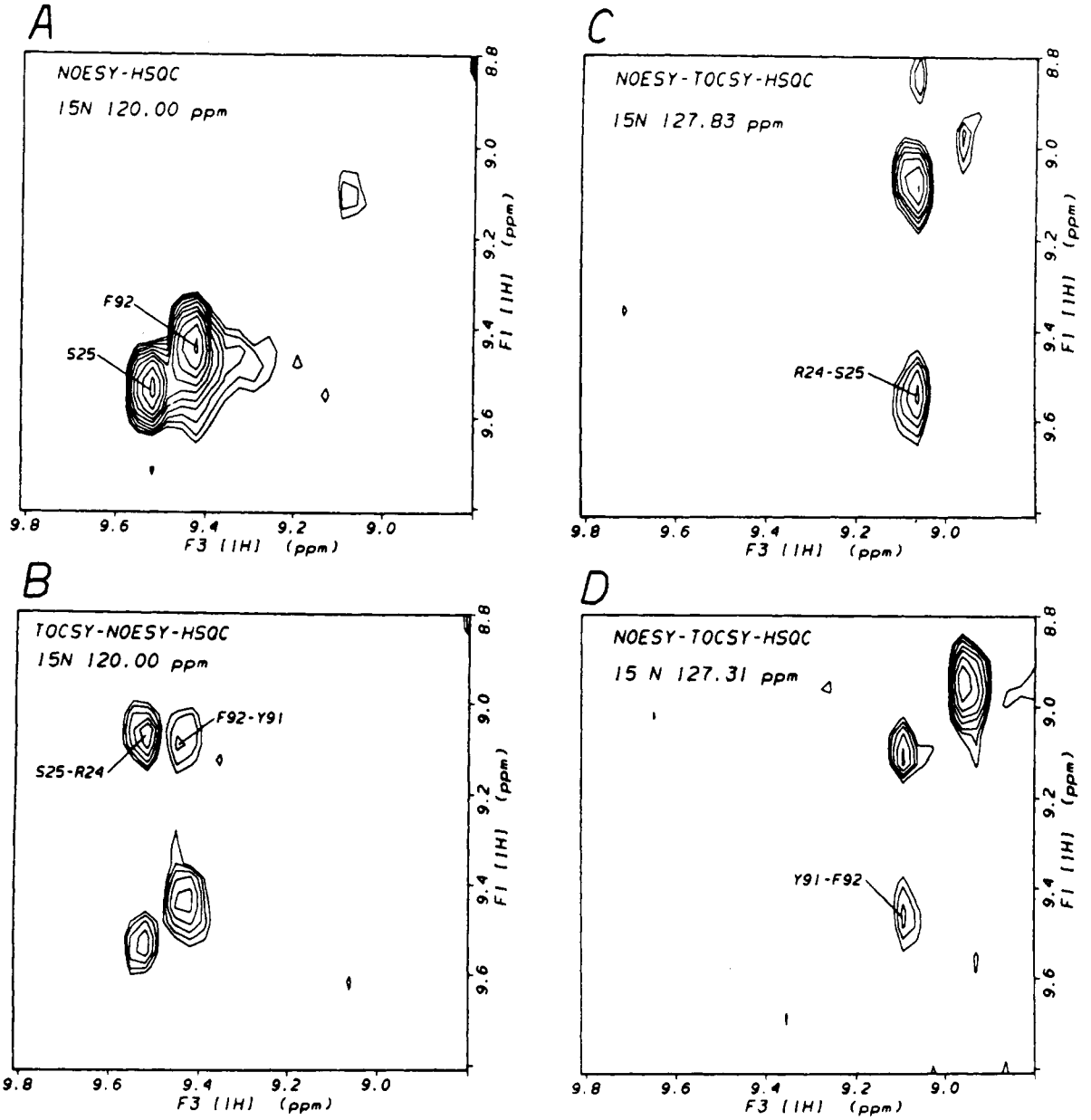

FIGURE 4: F_3, F_1 planes of the 600-MHz 3D spectra showing HN–HN connectivities between Arg^{24}-Ser^{25} and Tyr^{91}–Phe^{92}. (A) 3D NOESY–HSQC plane (δ ^{15}N = 120.00) containing Ser^{25} and Phe^{92} F_3, F_1 diagonal peaks. (B) 3D TOCSY–NOESY–HSQC plane (δ ^{15}N = 120.00). (C) 3D NOESY–TOCSY–HSQC plane (δ ^{15}N = 127.83) containing the Arg^{24} diagonal peak. (D) 3D NOESY–TOCSY–HSQC plane (δ ^{15}N = 127.31) containing the Tyr^{91} diagonal peak. Cross-peaks are labeled Res1(F_3)–Res2(F_1) in panels B, C, and D. Experimental conditions are the same as for Figure 1.

connectivities linking Asn^{35} to Thr^{36}, Phe^{60} to Ser^{61}, Ser^{94} to Gln^{95}, His^{98} to Val^{99}, and Pro^{101} to Thr^{102} all occur with lower than expected intensities. In general, the NOEs observed within the CDRs still reflect the crystalline conformations, albeit with reduced intensities in some instances. Strong evidence for the occurrence of similar conformations of CDR1, at least on average, in solution and in the crystalline state is also provided by the extreme downfield shift of the Asn^{33} HN resonance δ (12.51 ppm). In the 26-10 Fab X-ray structure, this proton is positioned between the aromatic rings of His^{31} and Tyr^{37} (P. Jeffrey, personal communication), consistent with the δ value reported here.

Medium-range and long-range NOEs which define contacts between elements of secondary structure (Wuthrich, 1986) were identified in the 2D NOESY, 3D NOESY–HSQC, and 3D NOESY–TOCSY–HSQC data. An example is given by Figure 6, which shows F_3, F_1 planes of the NOESY–HSQC (Figure 6A) and NOESY–TOCSY–HSQC (Figure 6B) spectra containing $d_{\alpha N}$ connectivities involving the HN resonance of Thr^7. In addition to intraresidue and sequential NOEs, the NOESY–HSQC spectrum contains a long-range connectivity to the Cys^{23} H^α resonance, which is one of the NOEs that define contacts between β-strands A and B. This NOE is absent from the corresponding region of the NOESY–TOCSY–HSQC spectrum, due to the relatively lower sensitivity of this experiment (Mueller et al., 1992). The Thr^7 HN and Pro^8 H^α resonances give rise to a cross-peak shown in Figure 6B. This connectivity is produced by NOESY-type magnetization transfer from the Pro^8 H^α resonance (F^1) to the H^α resonance of Thr^7, followed by TOCSY-type transfer to the Thr^7 HN resonance (F_3). (Note that the TOCSY transfer also increases the relative intensity of the Thr^7 intraresidue HN–H^α cross-peak.) Thus, close spatial proximity between the H^α protons of Thr^7 and Pro^8 is revealed, demonstrating that the intervening peptide bond is in the cis configuration, as expected on the basis of the X-ray structure. This was

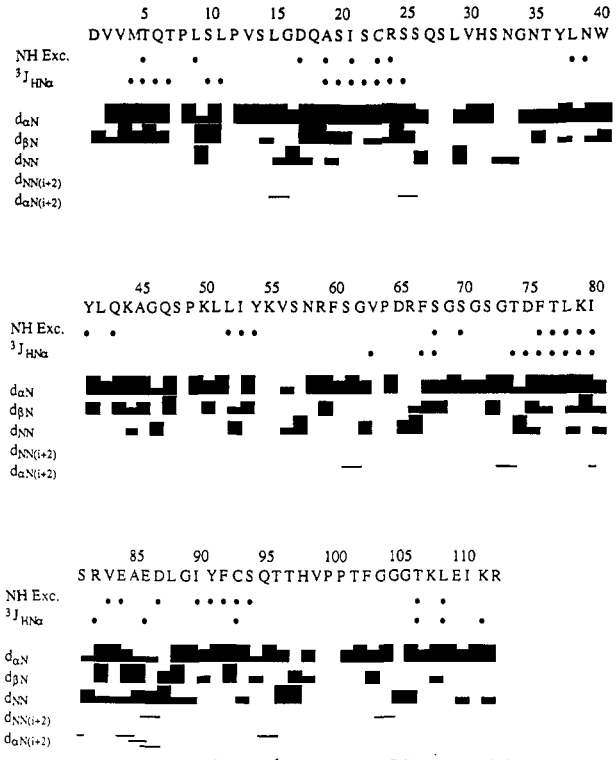

FIGURE 5: Sequential and $i,i+2$ ^1H NMR NOE connectivities observed for the 26-10 V_L domain. All indicated connectivities were observed in the 3D NOESY–HSQC spectrum. Sequential NOEs estimated to be strong, medium, and weak are distinguished by thick, medium, and thin solid horizontal bars between adjacent residues. Connectivities of the $i,i+2$ type are indicated by thin horizontal lines. $^3J_{\alpha HN}$ estimated to be >8 Hz and slowly exchanging amide HN protons are indicated by solid circles below the corresponding residues.

confirmed by subsequent location of the corresponding H^α–H^α cross-peak in the 2D NOESY spectra. The interstrand H^α–H^α proximities which occur in antiparallel β-sheets (Wuthrich, 1986) were derived from the 3D NOESY–TOCSY–HSQC and 2D NOESY spectra in an analogous manner.

The observed connectivities which define the 26-10 V_L domain secondary structure are depicted schematically in Figures 7 and 8. Figure 7 shows contacts involving β–strands A (N-terminal half), B, E, and D. Contacts between β-strands A (C-terminal half), G, F, C, C′ and C″ are shown in Figure 8. The NMR-derived features of secondary structure correspond very closely to features observed in the X-ray structure. All nine β-strands manifest the expected arrangement of interstrand contacts, which define the V_L domain framework (FR) regions (Coleman, 1988). Figure 7 shows NOEs revealing antiparallel proximities between residues 4 through 7 of strand A and residues 23 through 26 of strand B, between residues 18 through 25 of strand B and residues 75 through 81 of strand E, and between residues 76 through 81 of strand E and residues 66 through 72 of strand D. β-Turns consistent with the X-ray structure, involving residues 14 through 17, 24 through 27, and 72 through 75, have been identified. Connectivities are depicted in Figure 8 which delineate antiparallel proximities between residues 102 through 109 of strand G and residues 88 through 95 of strand F, between residues 89 through 95 of strand F and residues 38 through 44 of strand C, between residues 38 through 42 of strand C and residues 50 through 56 of strand C′, and between residue 53 of strand C′ and residue 60 of CDR2. NOEs which define parallel proximities between residues 10 through 13 of strand A and residues 108 through 112 of strand G are also shown. We note that strand A is interrupted by a *cis*-Pro turn (Pro^8). The expected β-turns involving residues 84 through 87 and 94 through 97 have been located. β-Bulges (Richardson et al., 1978) involving strand C′ residues 51 through 53 and strand G residues 104 through 106 are revealed by the data. These β-bulges are known to be conserved in both V_L and V_H domains (Chothia et al., 1985.

Regions of High Structural Stability. Slowly exchanging backbone HN protons are shown circled in Figures 7 and 8.

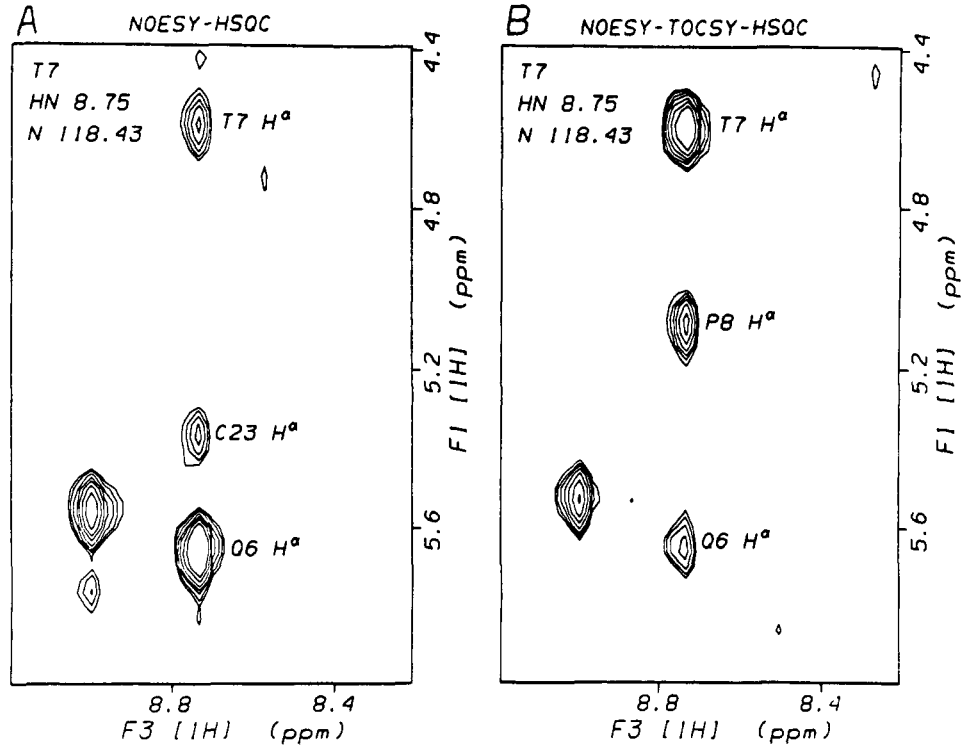

FIGURE 6: F_3, F_1 planes of 600-MHz 3D spectra showing connectivities from the HN proton of Thr^7 to various H^α protons. (A) 3D NOESY–HSQC spectrum (δ ^{15}N = 118.43). (B) 3D NOESY–TOCSY–HSQC spectrum (δ ^{15}N = 118.43). The various $HN(F_3)$–$H^\alpha(F_1)$ cross-peaks are labeled by the H^α residue. Experimental conditions are the same as for Figure 1.

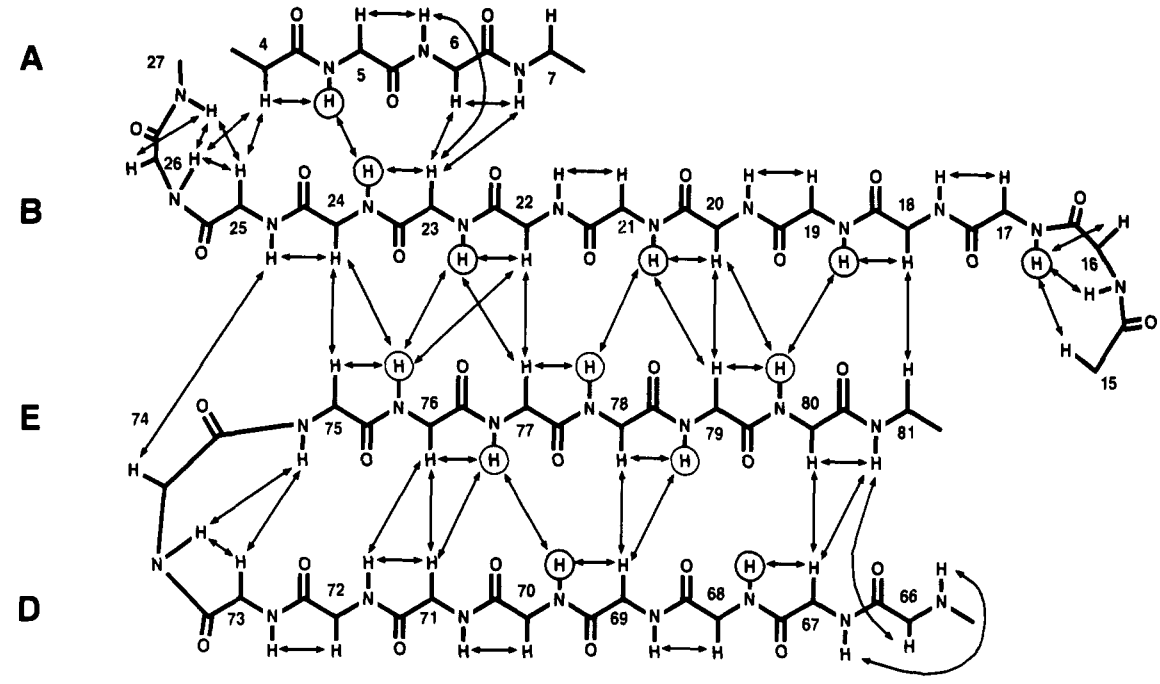

FIGURE 7: Schematic diagram illustrating NOE connectivities within and between β-strands A, B, E, and D. NOEs observed in 2D NOESY, 3D NOESY-HSQC, and/or 3D NOESY-TOCSY-HSQC spectra are indicated by arrows. For the latter experiment, HN-H^{α} cross-peaks reveal H^{α}-H^{α} NOE interactions, which are shown in the diagram (see text). Most of the H^{α}-H^{α} NOEs were subsequently identified in the 2D NOESY data. Slowly exchanging HN protons are circled.

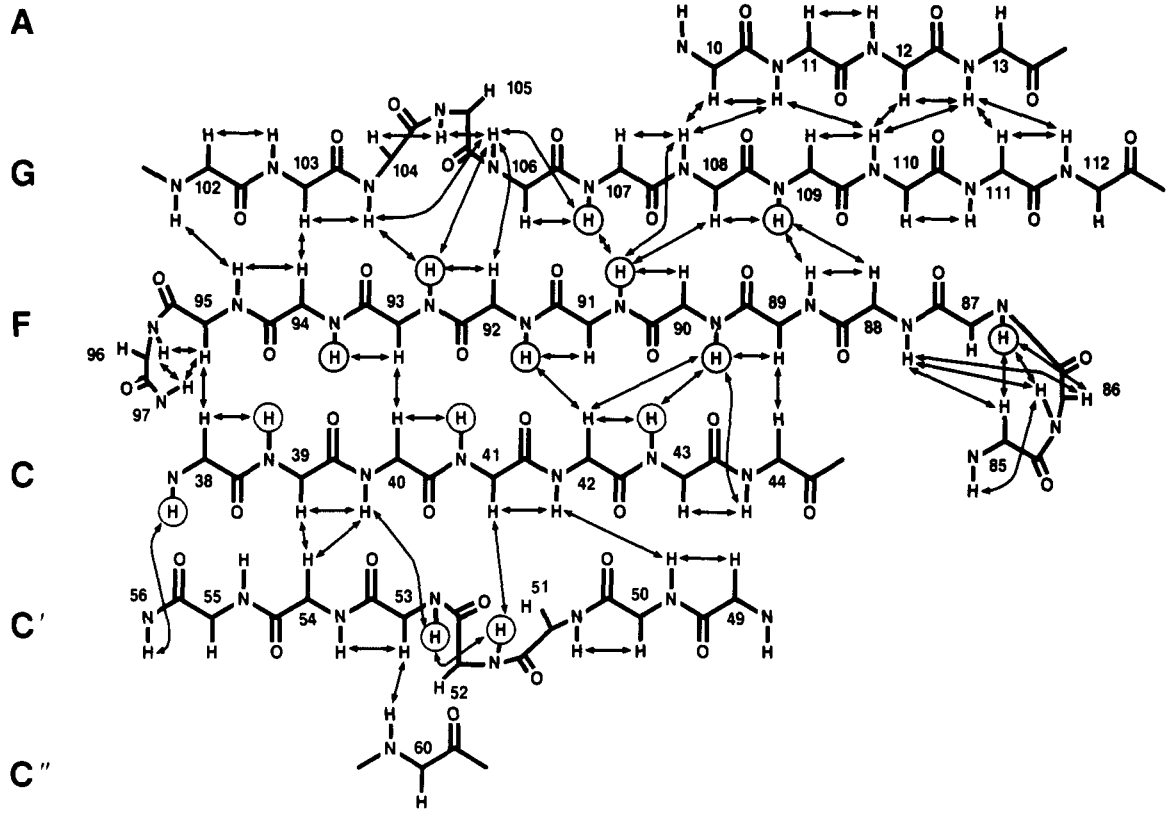

FIGURE 8: Schematic diagram illustrating NOE connectivities within and between β-strands A, G, F, C, C′, and C″. See the caption of Figure 7 for additional details.

These were identified by the presence of HN-H^{α} cross-peaks in a 2D TOCSY spectrum recorded over a time period extending from 12 to 24 h after the protein was dissolved in 99.96% ^2H_2O. The sites of slow exchange are distributed over most of the FRs. Strand B (part of FR1), strand C (part of FR2), and strands E and F (part of FR3) are found to be particularly stable. It is noteworthy that high stability is also indicated for the β-bulge feature of strand C′. Strands C, C′, F, and G, and portions of the CDRs, contribute to known V_L-V_H interfaces and to most known V_L-V_L interfaces (Schiffer et al., 1989; Colman, 1988; Stevens et al., 1988). Our results demonstrate that the elements of the 26-10 V_L domain secondary structure, including those encompassing residues involved in domain-domain interactions, are stable in the

Table I: ^1H and ^{15}N NMR Assignments for the 26-10 V_L Domain

residue	chemical shift (ppm)[a] N	HN	H^α	H^β	other
Asp^1			4.25	2.66, 2.55	
Val^2	123.62	8.80	3.62	1.84	H_3^γ 0.84, 0.50
Val^3	132.75	8.56	3.95	1.91	H_3^γ 1.02, 0.97
Met^4	129.04	9.01	5.41	1.86, 1.59	H^γ 2.38
Thr^5	121.80	9.66	4.61	4.08	H_3^γ 1.24
Gln^6	131.64	9.56	5.66	2.26, 2.10	H^γ 2.63, 2.54
Thr^7	118.42	8.75	4.60	4.13	H_3^γ 1.23
Pro^8			5.10		
Leu^9	121.48	8.76	4.65		
Ser^{10}	113.47	7.81	5.10	3.82, 3.79	
Leu^{11}	128.45	9.15	4.93	1.92	
Pro^{12}			5.21		
Val^{13}	120.47	9.17	4.75	2.19	H_3^γ 0.89, 0.72
Ser^{14}	119.29	8.58	4.84	4.19, 3.65	
Leu^{15}	123.67	8.66	3.83	1.73	
Gly^{16}	113.80	9.47	4.42, 3.33		
Asp^{17}	122.64	7.88	4.69	2.84	
Gln^{18}	117.83	8.24	4.80	2.00	H^γ 2.30; $H^\epsilon N$ 7.44, 6.78; N^ϵ 112.47
Ala^{19}	123.91	8.53	4.65	1.04	
Ser^{20}	116.07	7.74	5.30	3.59, 3.49	
Ile^{21}	125.58	9.02	4.44		
Ser^{22}	120.31	8.78	5.70	4.02, 3.92	
Cys^{23}	124.86	9.41	5.37	3.16, 2.99	
Arg^{24}	127.50	9.08	5.99	1.92, 1.83	H^γ 1.75; H^δ 3.23
Ser^{25}	120.00	9.53	5.69	3.72	
Ser^{26}	115.71	8.29	4.28		
Gln^{27}	116.93	7.30	4.62	2.11, 1.98	H^γ 2.15, 1.72; $H^\epsilon N$ 7.24, 6.62; N^ϵ 111.83
Leu^{29}	125.94	8.79	4.53	1.92	
Val^{30}	125.01	8.14	4.05		H_3^γ 1.03, 0.92
His^{31}	133.54	9.42	4.19	3.56, 3.17	H^2 7.79; H^4 7.31
Ser^{32}	126.29	8.06	4.18	3.89	
Asn^{33}	125.79	12.51			
Gly^{34}	108.96	8.59	4.44, 3.58		
Asn^{35}	120.52	8.57	4.70	2.73, 1.43	$H^\delta N$ 7.13, 6.81; N^δ 114.1
Thr^{36}	117.37	8.42	4.64	3.92	H_3^γ 0.96
Tyr^{37}	127.00	6.36	4.44	3.07	$H^{2,6}$ 7.16; $H^{3,5}$ 6.54
Leu^{38}	125.56	6.42	4.85		
Asn^{39}	123.86	8.96	5.56	2.57, 2.41	
Trp^{40}	118.33	9.00	5.52	3.15, 2.79	H^1N 11.04; N^1 133.90; H^2 6.60; H^5 7.42; H^6 6.85; H^7 7.06
Tyr^{41}	120.59	9.53	5.28	2.46, 2.25	
Leu^{42}	121.87	8.76	4.60	1.41, 1.15	
Gln^{43}	131.24	10.02	4.72	2.42	
Lys^{44}	130.23	8.66	4.58	1.94, 1.48	H^γ 1.71
Ala^{45}	124.79	8.48	4.13	1.39	
Gly^{46}	111.34	8.78	4.13, 3.78		
Gln^{47}	118.69	7.95	4.83	2.34, 2.00	
Ser^{48}	116.78	8.53	4.52	3.87, 3.76	
Pro^{49}			4.23		
Lys^{50}	125.65	8.89	4.57	1.87	
Leu^{51}	128.82	8.37	3.49		H_3^δ 0.98
Leu^{52}	125.05	8.87	4.82	1.53	
Ile^{53}	118.72	7.29	5.26	1.74	H_3^γ 0.74; H_3^δ 0.49
Tyr^{54}	123.64	9.34	5.75		$H^{2,6}$ 6.92; $H^{3,5}$ 6.73
Val^{56}	112.72	9.15	3.02		H_3^γ 1.05, 0.20
Ser^{57}	111.19	8.74	4.69		
Asn^{58}	123.80	8.19	4.69	1.86, 1.73	
Arg^{59}	125.58	9.01	4.69	1.88	
Phe^{60}	126.68	8.41	4.67	3.03	
Ser^{61}	120.59	6.54	4.03		
Gly^{62}	115.01	8.74	4.19, 3.69		
Val^{63}	126.05	7.91	4.39	2.42	H_3^γ 1.33, 1.10
Pro^{64}			4.70	2.25	
Asp^{65}	119.29	8.58	3.85	2.95	
Arg^{66}	114.92	6.91	4.28	1.75, 1.58	H^δ 3.22
Phe^{67}	120.46	7.70	5.00	3.00, 2.57	$H^{2,6}$ 7.18; $H^{3,5}$ 7.45; H^4 7.55
Ser^{68}	116.00	9.03	4.84	3.76	
Gly^{69}	112.03	9.06	5.34, 4.01		
Ser^{70}	116.21	9.05	4.87	4.00	
Gly^{71}	110.43	8.51	5.24, 3.93		
Ser^{72}	110.69	7.57	4.57	3.91, 3.84	
Gly^{73}	110.96	8.97	4.28, 3.56		
Thr^{74}	117.49	8.10	5.03		
Asp^{75}	123.47	7.02	5.23	2.57, 2.44	
Phe^{76}	122.50	8.84	5.38	3.67, 2.84	$H^{2,6}$ 6.94; $H^{3,5}$ 7.01; H^4 7.09
Thr^{77}	118.90	8.84	5.55	3.75	H_3^γ 1.03
Leu^{78}	130.65	8.70	4.50		H_3^δ 0.30
Lys^{79}	127.06	8.96	5.00	1.58, 1.45	H^γ 1.27, 1.18
Ile^{80}	124.61	8.66	4.40	1.33	H^γ 1.05, 0.56; H_3^γ 0.12; H_3^δ 0.38
Ser^{81}	122.69	9.01	4.07	3.82	
Arg^{82}	120.06	6.54	3.84	1.58	H^δ 3.17; $H^\epsilon N$ 7.35; N^ϵ 119.05
Val^{83}	124.61	8.66	3.74	1.84	H_3^γ 0.86, 0.81
Glu^{84}	130.49	9.33	4.72		
Ala^{85}	124.94	9.13	3.85	1.48	
Glu^{86}	114.86	8.56	4.28	2.12	
Asp^{87}	121.27	8.10	4.69	3.08, 2.99	
Leu^{88}	118.78	7.11	4.15	1.88, 1.64	
Gly^{89}	110.10	7.75	4.12, 3.96		
Ile^{90}	120.59	8.12	4.93	1.73	
Tyr^{91}	126.99	9.10	5.51	2.85	$H^{2,6}$ 6.89; $H^{3,5}$ 6.76
Phe^{92}	119.84	9.44	5.84	3.19, 2.83	
Cys^{93}	116.32	7.62	5.52	2.91, 2.81	
Ser^{94}	117.49	8.87	5.08	3.25, 2.97	
Gln^{95}	121.87	8.79	5.81		$H^\epsilon N$ 7.88, 7.56; N^ϵ 111.87
Thr^{96}	109.21	8.44	4.49		
Thr^{97}	123.62	7.99		3.95	H_3^γ 0.48
His^{98}	122.05	9.46	4.70	3.00, 2.59	H^2 7.87; H^4 6.48
Val^{99}	122.50	8.79	4.02	2.04	H_3^γ 1.00
Pro^{101}			4.75		
Thr^{102}	110.69	7.59	4.85		
Phe^{103}	121.00	8.87	5.24	3.35	
Gly^{104}	109.09	9.06	4.42		
Gly^{105}	105.18	8.54	4.24, 4.06		
Gly^{106}	107.10	7.02	4.12, 3.90		
Thr^{107}	119.54	8.34	4.84		H_3^γ 1.02
Lys^{108}	129.37	8.48	4.66	1.94	
Leu^{109}	133.54	9.12	5.06	2.28	
Glu^{110}	125.32	8.14	4.87		
Ile^{111}	122.12	8.35	4.84		
Lys^{112}	129.51	8.31	4.21	1.66, 1.34	
Arg^{113}	131.24	8.10	4.23		H^δ 3.20; $H^\epsilon N$ 7.22; N^ϵ 119.21

[a] The ^1H chemical shift values (±0.02 ppm) were derived from 3D TOCSY–HSQC and (for the aromatic ring protons) 2D TOCSY spectra recorded at pH 5.5, 30 °C, while the ^{15}N chemical shift values (±0.10 ppm) for 103 residues were derived from the 2D HSQC spectrum recorded under the same conditions. The Phe^{103} ^{15}N chemical shift was derived from the 3D TOCSY–HSQC spectrum. Reported Arg N^ϵ chemical shift values refer to their folded locations.

absence of quaternary interactions. The Trp^{40} side-chain H^1N proton also exchanges slowly with solvent. It is of interest to note that this conserved residue is buried within the protein core, yet there are no suitably positioned H-bond acceptor groups near the H^1N proton (P. Jeffrey, personal communication). Indeed, there is a cavity present adjacent to this proton. We suggest that the Trp^{40} H^1N proton may be involved in a bridging H-bond interaction with a buried water molecule. In any case, the Trp^{40} environment is demonstrated to be highly stable.

The results described above suggest that no *major* changes in the V_L domain tertiary structure occur upon V_L/V_H asso-

ciation. As such changes are expected to induce strain within the domains, and consequently yield an unfavorable enthalpic contribution to the free energy of association, their absence favors stronger association. A relatively high degree of rigidity would favor associations between domains with well-matched surface features, and would tend to disfavor induced fit type association mechanisms. Thus, if V_L/V_L association requires a greater degree of induced fit than V_H/V_L association, there may be a correlation between the observations that the 26-10 V_L domain shows relatively strong affinity for its complementary V_H domain (Anthony et al., 1992) but apparently little or no self-association.

Concluding Remarks

We have obtained ^1H assignments for 110 of the 113 26-10 V_L residues. Backbone ^{15}N assignments for 104 residues have also been reported. The utility of 3D TOCSY–NOESY–HSQC and NOESY–TOCSY–HSQC spectra for assigning a uniformly ^{15}N-enriched protein, and in particular a protein containing a large amount of β-sheet secondary structure, has been demonstrated. At the qualitative level, no difference in secondary structure elements between the isolated V_L domain in solution and the V_L domain as part of the crystalline 26-10 Fab–digoxin complex could be discerned. The CDR loops also appear to adopt similar solution and crystalline conformations, but they may have enhanced flexibility relative to the FRs. The FR β-strands are shown to be rather stable, particularly strands B, C, E, and F. A possible role for intradomain stability in determining the strength of domain–domain interactions has been suggested.

A quantitative understanding of factors leading to stable V_H/V_L association and to the formation of stable Fv–antigen complexes will require high-resolution structural information for isolated variable domains, and for antigen-free and antigen-bound Fv fragments. Detailed knowledge of the degree of dynamic flexibility in these various forms is also required, as any attempt to estimate strain and conformational entropy loss upon association depends on this information. The results reported here represent an initial effort, using high-resolution NMR methods, to address these issues.

Acknowledgments

We thank Dr. P. D. Jeffrey and Dr. S. Sheriff for providing us with V_L coordinates extracted from the 26-10 Fab X-ray structure and for many illuminating discussions regarding antibody domain structure. Assistance in the acquisition of NMR data provided by Dr. M. McCoy, and assistance in NMR data processing provided by Dr. M. Friedrichs, is gratefully acknowledged. We also thank Dr. R. Beckman for carefully reading the manuscript and Dr. E. Haber for his continuing input to this project.

Registry No. Digoxin, 20830-75-5.

References

Anthony, J., Near, R., Wong, S., Iida, E., Ernst, E., Wittekind, M., Haber, E., & Ng, S.-C. (1992) *Mol. Immunol.* (in press).

Baldwin, E., & Schultz, P. G. (1989) *Science 245*, 1104–1107.

Bax, A., & Davis, D. G. (1985) *J. Magn. Reson. 65*, 355–360.

Bhat, T. N., Bentley, G. A., Fischmann, T. O., Boulot, G., & Poljak, R. J. (1990) *Nature 347*, 483–485.

Bird, R. E., Hardman, K. D., Jacobson, J. W., Johnson, S., Kaufman, B. M., Lee, S., Lee, T., Pope, S. H., Riordan, G. S., & Whitlow, M. (1988) *Science 242*, 423–426.

Bodenhausen, G., & Ruben, D. J. (1980) *Chem. Phys. Lett. 69*, 185–188.

Bodenhausen, G., Kolger, H., & Ernst, R. R. (1984) *J. Magn. Reson. 58*, 370–388.

Braunschweiler, L., & Ernst, R. R. (1983) *J. Magn. Reson. 53*, 521–528.

Brown, S. C., Weber, P. L., & Mueller, L. (1988) *J. Magn. Reson. 77*, 166–169.

Brünger, A. T. (1990) *X-PLOR (Version 2.1) Manual*, Yale University Press, New Haven, CT.

Chaudhary, V. K., Queen, C., Junghans, R. P., Waldmann, T. A., Fitzgerald, D. J., & Pastan, I. (1989) *Nature 339*, 394–397.

Chothia, C., & Lesk, A. M. (1985) *Trends Biochem. Sci. 10*, 116–118.

Colcher, D., Bird, R., Roselli, M., Hardman, K. D., Johnson, S., Pope, S., Dodd, S. W., Pantaliano, M. W., Milenic, D. E., & Schlom, J. (1990) *J. Natl. Cancer Inst. 82*, 1191–1197.

Colman, P. M. (1988) *Adv. Immunol. 43*, 99–132.

Davies, D. R., Padlan, E. A., & Sheriff, S. (1990) *Annu. Rev. Biochem. 59*, 439–473.

Edmondson, A. B., Ely, K. R., & Herron, J. N. (1984) *Mol. Immunol. 21*, 561–576.

Fesik, S. W., & Zuiderweg, E. R. P. (1990) *Q. Rev. Biophys. 23*, 97–131.

Gibbs, R. A., Posner, B. A., Filpula, D. R., Dodd, S. W., Finkelmann, M. A. J., Lee, T. K., Wroble, M., Whitlow, M., & Benkovic, S. J. (1991) *Proc. Natl. Acad. Sci. U.S.A. 88*, 4001–4004.

Givol, D. (1991) *Mol. Immunol. 28*, 1379–1386.

Glockshuber, R., Malia, M., Pfitzinger, I., & Plückthun, A. (1990) *Biochemistry 29*, 1362–1367.

Griesinger, C., Otting, G., Wüthrich, K., & Ernst, R. R. (1988) *J. Am. Chem. Soc. 110*, 7870–7872.

Huston, J. S., Levinson, D., Mudgett-Hunter, M., Tai, M., Novotny, J., Margolies, M. N., Ridge, R. J., Bruccoleri, R. E., Haber, E., Crea, R., & Oppermann, H. (1988) *Proc. Natl. Acad. Sci. U.S.A. 85*, 5879–5883.

Kay, L. E., Ikura, Mlk Tschudin, R., & Bax, A. (1990) *J. Magn. Reson. 89*, 496–514.

Kishida, F., Azuma, T., & Hamaguchi, K. (1975) *J. Biochem. 77*, 481–491.

Kumar, A., Ernst, R. R., & Wüthrich, K. (1980) *Biochem. Biophys. Res. Commun. 95*, 1–6.

Macura, S., & Ernst, R. R. (1980) *Mol. Phys. 41*, 95–117.

Marion, D., Ikura, M., & Bax, A. (1989) *J. Magn. Reson. 84*, 425–428.

McManus, S., & Riechmann, L. (1991) *Biochemistry 30*, 5851–5857.

Mei, S., Mody, B., Eklund, S. H., & Paul, S. (1991) *J. Biol. Chem. 266*, 15571–15574.

Mueller, L., & Ernst, R. R. (1979) *Mol. Phys. 38*, 963–992.

Mueller, L., Campbell-Burk, S., & Domaille, P. (1992) *J. Magn. Reson. 96*, 408–415.

Norwood, T. J., Boyd, J., Heritage, J. E., Soffe, N., & Campbell, I. D. (1990) *J. Magn. Reson. 87*, 488–501.

Otting, G., Widmer, H., Wagner, G., & Wüthrich, K. (1986) *J. Magn. Reson. 66*, 187–193.

Pantoliano, M. W., Bird, R. E., Johnson, S., Asel, E. D., Dodd, S. W., Wood, J. F., & Hardmann, K. D. (1991) *Biochemistry 30*, 10117–10125.

Rance, M., Sorensen, O. W., Bodenhausen, G., Wagner, G., & Ernst, R. R. (1983) *Biochem. Biophys. Res. Commun. 69*, 979-987.
Richardson, J. S., Getzoff, E. D., & Richardson, D. C. (1978) *Proc. Natl. Acad. Sci. U.S.A. 75*, 2574-2578.
Schiffer, M., Ainsworth, C., Xu, Z. B., Carperos, W., Olsen, K., Solomon, A., Stevens, F. J., & Chang, C. H. (1989) *Biochemistry 28*, 4066-4072.
Schildbach, J. F., Panka, D. J., Parks, D. R., Jager, G. C., Herzenberg, L. A., Mudgett-Hunter, M., Haber, E., & Margolies, M. N. (1991) *J. Biol. Chem. 266*, 4640-4647.
Shaka, A. J., Keeler, J., Frenkiel, T., & Freeman, R. (1983) *J. Magn. Reson. 52*, 335.
States, D. J., Haberkorn, R. A., & Ruben, D. J. (1982) *J. Magn. Reson. 48*, 286-292.
Stevens, F. J., Westholm, F. A., Solomon, A., & Schiffer, M. (1980) *Proc. Natl. Acad. Sci. U.S.A. 77*, 1144-1148.
Stevens, F. J., Chang, C. H., & Schiffer, M. (1988) *Proc. Natl. Acad. Sci. U.S.A. 85*, 6895-6899.
Stevens, F. J., Solomon, A., & Schiffer, M. (1991) *Biochemistry 30*, 6803-6805.
Takahashi, H., Odaka, A., Kawaminami, S., Matsunga, C., Kato, K., Shimada, I., & Arata, Y. (1991) *Biochemistry 30*, 6611-6619.
Ward, E. S., Guessow, D., Griffiths, A. D., Jones, P. T., & Winter, G. (1989) *Nature 341*, 544-546.
Wright, P. E., Dyson, H. J., Lerner, R. A., Riechmann, L., & Tsang, P. (1990) *Biochem. Pharmacol. 40*, 83-88.
Wüthrich, K. (1986) *NMR of Proteins and Nucleic Acids*, John Wiley & Sons, New York.

Glycosylinositol Phospholipid Anchors of the Scrapie and Cellular Prion Proteins Contain Sialic Acid†

Neil Stahl,‡ Michael A. Baldwin,‡ Rolf Hecker,‡ Keh-Ming Pan,‡ Alma L. Burlingame,§ and Stanley B. Prusiner*,‡,∥

Departments of Neurology, Pharmaceutical Chemistry, and Biochemistry and Biophysics, University of California, San Francisco, California 94143

Received October 3, 1991; Revised Manuscript Received January 31, 1992

ABSTRACT: The only identified component of the scrapie prion is PrP^{Sc}, a glycosylinositol phospholipid (GPI)-linked protein that is derived from the cellular isoform (PrP^{C}) by an as yet unknown posttranslational event. Analysis of the PrP^{Sc} GPI has revealed six different glycoforms, three of which are unprecedented. Two of the glycoforms contain *N*-acetylneuraminic acid, which has not been previously reported as a component of any GPI. The largest form of the GPI is proposed to have a glycan core consisting of Manα-Manα-Man-(NeuAc-Gal-GalNAc-)Man-GlcN-Ino. Identical PrP^{Sc} GPI structures were found for two distinct isolates or "strains" of prions which specify different incubation times, neuropathology, and PrP^{Sc} distribution in brains of Syrian hamsters. Limited analysis of the PrP^{C} GPI reveals that it also has sialylated glycoforms, arguing that the presence of this monosaccharide does not distinguish PrP^{C} from PrP^{Sc}.

Recent research has substantiated the unusual molecular nature of the pathogens causing scrapie and other transmissible neurodegenerative disorders, but their exact structure and replicative mechanism remain enigmatic (Prusiner, 1991). These pathogens were named prions (Prusiner, 1982) because diverse experimental approaches have consistently failed to reveal the participation of a nucleic acid in their transmission to inoculated recipients (Alper et al., 1967; Bellinger-Kawahara et al., 1987, 1988; Duguid et al., 1988; Oesch et al., 1988; Meyer et al., 1991). In contrast, numerous results establish that a host-encoded protein designated PrP^{Sc} [1] is a component of the scrapie prion (Bolton et al., 1982; McKinley et al., 1983; Gabizon et al., 1988; Scott et al., 1989; Prusiner et al., 1990; Hsiao et al., 1989, 1990). PrP^{Sc} is a disease-specific isoform of a normal cellular protein of unknown function denoted PrP^{C} (Oesch et al., 1985; Basler et al., 1986). In addition to scrapie, prions containing PrP are implicated in the transmissible human neurodegenerative diseases kuru, Creutzfeldt-Jakob disease (CJD), and Gerstmann-Sträussler-Scheinker disease (GSS) (Gajdusek, 1977; Masters et al., 1981; Prusiner, 1987). Several varieties of CJD and GSS are unique in that the disease occurs in families with an autosomal dominant pattern

† This work was supported by grants from the NIH (NS14069, AG02132, NS22786, and AG08967) and the American Health Assistance Foundation as well as by gifts from the Sherman Fairchild Foundation and National Medical Enterprises. R.H. was supported by a fellowship from the European Molecular Biology Organization. The Bio-organic, Biomedical Mass Spectrometry Resource (A. L. Burlingame, Director) was supported by National Institutes of Health National Center for Research Resources Grant RR01614 and by National Science Foundation Biological Instrumentation Program Grant DIR8700766.

* To whom correspondence should be addressed at the Department of Neurology, HSE-781, University of California, San Francisco, CA 94143-0518.
‡ Department of Neurology.
§ Department of Pharmaceutical Chemistry.
∥ Department of Biochemistry and Biophysics.

[1] Abbreviations: PrP^{Sc}, scrapie isoform of the prion protein; PrP^{C}, cellular isoform of the prion protein; PrP 27-30, N-terminally truncated form derived from PrP^{Sc} by limited proteolysis; GPI, glycosylinositol phospholipid; PIPLC, phosphatidylinositol-specific phospholipase C; K12-GPI, C-terminal GPI-linked peptide purified after digestion of PrP with endoproteinase Lys-C and PIPLC; LSIMS, liquid secondary ion mass spectrometry; ESP, electrospray mass spectrometry; CE, capillary electrophoresis; HPAE, high-pH anion exchange; NANA, *N*-acetylneuraminic acid; GlcN, glucosamine; GalNAc, *N*-acetylgalactosamine; Ino, inositol; Man, mannose; Gal, galactose.

0006-2960/92/0431-5043$03.00/0